ORIGINAL ARTICLE

# Cholesterol-tuned liposomal membrane rigidity directs tumor penetration and anti-tumor effect

Hangyi Wu[a,b], Miaorong Yu[b], Yunqiu Miao[b], Shufang He[b], Zhuo Dai[b],
Wenyi Song[b], Yuan Liu[b], Sha Song[b], Ejaj Ahmad[b], Dongkai Wang[a,*],
Yong Gan[b,**]

[a]Department of Pharmaceutics, Shenyang Pharmaceutical University, Shenyang 117004, China
[b]Shanghai Institute of Materia Medica, Chinese Academy of Sciences, Shanghai 201203, China

**Abstract**   Recently, liposomes have been widely used in cancer therapeutics, but their anti-tumor effects are suboptimal due to limited tumor penetration. To solve this problem, researchers have made significant efforts to optimize liposomal diameters and potentials, but little attention has been paid to liposomal membrane rigidity. Herein, we sought to demonstrate the effects of cholesterol-tuned liposomal membrane rigidity on tumor penetration and anti-tumor effects. In this study, liposomes composed of hydrogenated soybean phospholipids (HSPC), 1,2-distearoyl-$sn$-glycero-3-phosphoethanolamine-$N$-[methoxy(polyethylene glycol)-2000] (DSPE-PEG$_{2000}$) and different concentrations of cholesterol were prepared. It was revealed that liposomal membrane rigidity decreased with the addition of cholesterol. Moderate cholesterol content conferred excellent diffusivity to liposomes in simulated diffusion medium, while excessive cholesterol limited the diffusion process. We concluded that the differences of the diffusion rates likely stemmed from the alterations in liposomal membrane rigidity, with moderate rigidity leading to improved diffusion. Next, the $in\ vitro$ tumor penetration and the $in\ vivo$ anti-tumor effects were analyzed. The results showed that liposomes with moderate rigidity gained excellent tumor penetration and enhanced anti-tumor effects. These findings illustrate a feasible and effective way to improve tumor penetration and therapeutic efficacy of liposomes by changing the cholesterol content, and highlight the importance of liposomal membrane rigidity.

---

*Corresponding author at: Shenyang Pharmaceutical University, 26 Huatuo Street, High-tech Industrial Development Zone, Benxi 117004, Liaoning, China.
**Corresponding author at: Shanghai Institute of Materia Medica, Chinese Academy of Sciences, 501 Haike Road, Shanghai 201203, China. Tel./fax: +86 021 20231000 1424.
   E-mail addresses: wangycsyphu@126.com (Dongkai Wang), ygan@simm.ac.cn (Yong Gan).

## 1. Introduction

The development of anti-tumor compounds has gained momentum in the last decade, but their *in vivo* therapeutic effects remain limited[1]. To achieve significant anti-tumor effects *via* intravenous injection, drug carriers are required to circulate in the blood, leak out from peri-tumoral vessels, penetrate deeply into tumor tissues, and be internalized by tumor cells[2,3]. However, for certain recalcitrant solid tumors, cellular and extracellular elements interweave and mutually facilitate to compose dense cross-linked structures. As a result, drug carriers are enriched around the tumor tissues due to the enhanced permeability and retention (EPR) effect and are mostly trapped on the surface of solid tumor tissues, leading to poor anti-tumor effects[4,5]. Therefore, tumor penetration is considered the most significant "rate-limiting step" in cancer treatment[6,7], and innovative strategies that enhance the tumor penetration of drug carriers are urgently needed.

Extensive research on liposomes has proven their utility in drug delivery, and liposomes are considered one of the most promising and versatile drug carriers for cancer therapeutics[8]. The Food and Drug Administration (FDA) has already approved some liposomal preparations for clinical use, such as Doxil® and Onivyde®, while others are under active clinical investigation. Recently, modification of liposomal surface[9] and the development of environmentally sensitive liposomes[10] have become hot topics for enhancing the utility of liposomes, and some liposomes have shown significant anti-tumor potential. Compared to studies on specific modifications, investigation of the basic properties of liposomes, such as diameter[11] and zeta potential[12], may prove particularly beneficial. The rigidity of liposomes is one of the most important properties affecting their drug delivery effectiveness. Specifically, the increase in rigidity may result in the enhanced colloidal stability, drug release, hydrophobicity, and cellular uptake of liposomes[13–18]. However, for liposomes to find use in treating recalcitrant solid tumors, it is also essential to study the effect of liposomal rigidity on tumor penetration[1].

Studies on particle rigidity, such as those on core-shell nanoparticles[19] and internal-modified nanolipogels[15], were required to build a complex model for establishing the rigidity gradient internal modified nanolipogels. However, these carriers require complicated preparation processes and have not been proven viable for commercial scale-up production. Cholesterol, a crucial constituent of liposomes, has not received adequate attention. In addition to its well-known functions in liposomes, such as the enhancement in membrane ordering[20] and liposomal stability[21], cholesterol also has significant influence on the rigidity of liposomes[22] and can affect liposomal cellular uptake[23]. Furthermore, it is more convenient and biocompatible to change the cholesterol content of liposomes, compared to liposomal surface modifications and environmentally sensitive modifications. However, there are some opposite results about the effects of cholesterol on membrane rigidity in the reported studies. For example, when the lipid membrane was composed of cholesterol and stearoyloleoylphosphatidylcholine (SOPC) (or dimyristoylphosphatidylcholine (DMPC) or palmitoyloleoylphosphatidylcholine (POPC)), the membrane rigidity increased with the content of cholesterol[24,25]. However, cholesterol content could not affect the membrane rigidity of liposomes composed of dioleoylphosphatidylcholine (DOPC)[25,26]. On the contrary, for liposomes with egg sphingomyelin (SM), the membrane rigidity was found to be decreased with the content of cholesterol increased[22,27]. The liposomal membrane rigidity is predominantly determined by the phase state of the membrane, which decreased in the following order: solid phase > solid-liquid coexisting phase > liquid phase[28]. While, the effect of cholesterol on the membrane phase state as well as liposomal membrane rigidity is phospholipid selective[26,27]. In addition to the membrane phase state, this effect may also depend on several multiple factors, such as the lipid individual molecular architecture, acyl chain length and unsaturation, and probably the lipid interfacial region[26]. In our study, we selected the classic lipid—HSPC, which is a component of Doxil® (the first commercially available liposome and commonly used as the positive control group in the anti-tumor researches), as the model to reveal the effect of membrane rigidity on liposomal tumor penetration and anti-tumor effect.

Herein, liposomes were prepared with hydrogenated soybean phospholipids (HSPC), 1,2-distearoyl-*sn*-glycero-3-phosphoethanolamine-*N*-[methoxy(polyethylene glycol)-2000] (DSPE-PEG$_{2000}$) and different amounts of cholesterol, and their membrane rigidity was characterized using atomic force microscopy (AFM). Next, the diffusion processes of these preparations were examined by multiple-particle tracking technology, and their cellular uptake properties were measured. Finally, BxPC-3&HPaSteC co-cultured three-dimensional (3D) tumor spheroids and BxPC-3&HPaSteC tumor-bearing nude mice were constructed to explore the *in vitro* tumor penetration and *in vivo* anti-tumor effects of the different liposomal preparations. The results suggested that liposomal membrane rigidity decreased when the cholesterol content was increased, while liposomes with moderate membrane rigidity exhibited better tumor penetration and therapeutic effects, which might be beneficial for the treatment of recalcitrant solid tumors.

## 2. Materials and methods

### 2.1. Materials

Doxorubicin hydrochloride (DOX) was a generous gift from Shanghai Pharma (Shanghai, China). HSPC, cholesterol, DSPE-PEG$_{2000}$ and 1,2-distearoyl-*sn*-glycero-3-phosphoethanolamine-*N*-mPEG$_{2000}$ (DSPE-PEG$_{2000}$-FITC) were purchased from Shanghai Advanced Vehicle Technology Pharmaceutical Co., Ltd. (Shanghai, China). 3-[4,5-Dimethylthiazol-2-yl]-2,5-diphenyl tetrazolium bromide (MTT) and 4′,6-diamidino-2-phenylindole (DAPI) and were all bought from Sigma–Aldrich (St. Louis, MO, USA). Sephadex G-50 was obtained from Shanghai Jianglai Biological Technology Co., Ltd. (Shanghai, China). RPMI 1640 medium, Dulbecco's modified Eagle's medium (DMEM), fetal bovine serum (FBS), penicillin/streptomycin, and trypsin–EDTA solution (0.25% trypsin with 0.53 mmol/L EDTA) were purchased from Life Technologies Co. (Grand Island, NY, USA). All other chemicals and reagents were obtained from Sinopharm Chemical Reagent Co., Ltd. (Shanghai, China).

### 2.2. Preparation of liposomes

Drug-loaded liposomes were prepared by the thin-film hydration and ammonium sulfate gradient drug-loading method. The lipid compositions of the different liposomes used in this study are listed in Table 1. Briefly, 5.4 mg of total lipid was dissolved in chloroform in a round-bottom flask. A lipid thin-film was formed by gently evaporating at 37 °C using a rotary evaporator. Then, the film was hydrated with 1 mL of an ammonium sulfate solution (250 mmol/L) for 30 min at 60 °C. The resulting preparations were extruded through 100 nm polycarbonate membranes. To establish the ammonium sulfate gradient, the extruded liposome sample was passed through a Sephadex-50 column pre-equilibrated with a sucrose solution (0.3 mol/L). Then, 0.7 mg of DOX and the eluted liposomes were

**Table 1**   Characterization of liposomes with different cholesterol content.

| Preparation | Composition (molar ratio)[a] | Composition (mass ratio)[a] | EE (%) of DOX[b] | LC (%) of DOX[b] | Diffusivity ($\mu m^2$/s) | Ratio of diffusivity | Young's modulus (MPa)[b] |
|---|---|---|---|---|---|---|---|
| Lip1 | 97.5:/:2.5 | 4.95:/:0.45 | 92.5 ± 1.2 | 10.6 ± 0.2 | 0.14 | 1 | 53.3 ± 4.5 |
| Lip2 | 77.5:20.0:2.5 | 4.35:0.55:0.50 | 94.2 ± 1.4 | 10.8 ± 0.2 | 0.75 | 5.4 | 33.9 ± 3.6 |
| Lip3 | 67.5:30.0:2.5 | 4.00:0.87:0.53 | 95.7 ± 1.5 | 11.0 ± 0.2 | 1.55 | 11.1 | 28.2 ± 3.4 |
| Lip4 | 57.5:40.0:2.5 | 3.60:1.24:0.56 | 96.8 ± 1.7 | 11.1 ± 0.2 | 1.13 | 8.1 | 21.7 ± 4.2 |
| Lip5 | 47.5:50.0:2.5 | 3.17:1.64:0.60 | 95.0 ± 1.2 | 10.9 ± 0.1 | 0.35 | 2.5 | 11.5 ± 3.1 |
| Lip6 | 56.3:38.4:5.3 | 3.24:1.08:1.08 | 96.7 ± 1.6 | 11.0 ± 0.2 | 1.72 | 12.2 | 23.8 ± 5.6 |

EE (%), entrapment efficiency; LC (%), drug loading content. /, not applicable.
[a]Compositions of preparations are shown as HSPC:cholesterol:DSPE-PEG$_{2000}$.
[b]Data are presented as the mean ± SD ($n$ = 3).

co-incubated at 60 °C for 1 h. The liposome–drug mixture was routinely subjected to a Sephadex-50 column equilibrated with 4-(2-hydroxyethyl)-1-piperazineëthanesulfonic acid (HEPES) buffer to remove any unencapsulated drug. Finally, the liposomes were concentrated using ultrafiltration tubes. The FITC-labeled liposomes were hydrated with distilled water. In the preparation of FITC-labeled liposomes, cholesterol, HSPC, DSPE-PEG$_{2000}$ and DSPE-PEG$_{2000}$-FITC was used. The phospholipids were added by the molar ratio. For example, Lip1 was composed by 97.5% HSPC and 2.5% total PEG ($M_{DSPE-PEG2000}$ + $M_{DSPE-PEG2000-FITC}$) (mol/mol). The concentration of FITC was 1 μg/mL.

The actual contents and compositions of the liposomes were measured by using high performance liquid chromatography (HPLC) with an evaporative light-scattering detector (ELSD)[29]. In brief, after extruded through 100 nm polycarbonate membranes, the liposomes were placed in a dialysis membrane bag (MW 14,000 Da) to remove the free lipid. Then, the remaining liposomes were measured by HPLC with ELSD. The recovery ratios of different compositions were calculated by Eq. (1):

$$\text{Recovery (\%)} = \frac{\text{Recovered concentration (μg/mL)}}{\text{Feeding concentration (μg/mL)}} \times 100 \quad (1)$$

The entrapment efficiency (EE) and loading content (LC) of DOX of different liposomes were determined via a HPLC assay and were calculated using Eqs. (2) and (3), respectively:

$$\text{EE (\%)} = M_1 / (M_0 + M_1) \times 100 \quad (2)$$

$$\text{LC (\%)} = M_1 / (M_L + M_1) \times 100 \quad (3)$$

where $M_0$ represents the weight of the free drug, $M_1$ represents the weight of the drug in liposomes, and $M_L$ represents the weight of the total lipid in each preparation.

### 2.3.   Characterization of liposomes

The average size and zeta potential of the different preparations were determined by dynamic light scattering (DLS) at 25 °C in a Nano ZS zetasizer (Malvin, UK). The morphologies of the different preparations were observed using a Cryo-transmission electron microscopy (Cryo-TEM, Tecnai 12 electron microscope, USA).

Atomic force microscopy (AFM) was used to characterize the membrane rigidity of the liposomes. Briefly, force measurement was performed using a Bio-Fast Scan scanning probe microscope in Peak Force QNM imaging mode. The liposomes (drug free) were dropped onto a freshly cleaved mica surface, air-dried at room temperature, and then placed in an 85% humidity chamber

for 1 h. The samples were imaged with a scan rate of 1 Hz. A cantilever with a deflection sensitivity of 75 nm/V and a tip with a spring constant of 0.53 N/m were applied. The Young's modulus of each NP was processed using Nanoscope Analysis software (Bruker, USA).

### 2.4.   In vitro drug release from liposomes

In vitro drug release was assessed by the dialysis method using dialysis membranes in phosphate buffered saline (PBS). In brief, liposomes were placed in a dialysis membrane bag (MW 14,000 Da) and incubated in 50 mL of PBS separately at pH 7.4 in a shaking water bath incubator at 37 °C in the dark. DOX solution was used as control. At pre-determined time intervals, 1 mL of the release medium was taken out and replenished with 1 mL of fresh PBS. The released DOX was determined by HPLC. All experiments were performed in triplicate. The accumulative percentage drug release (Er) was calculated using Eq. (4):

$$\text{Er (\%)} = (V_r C_i + V_0 C_n) / M_{Dox} \times 100 \quad (4)$$

where $M_{DOX}$ represents the amount of DOX loaded in the liposomes, $V_0$ represents the total volume of the release medium, $V_r$ represents the volume of release medium taken out at each time point, $C_i$ represents the concentration of DOX in the $i$th aliquot that was removed, and $C_n$ represents the concentration of DOX in the last aliquot that was removed.

### 2.5.   Multiple-particle tracking

The in vitro diffusion properties of various liposomal preparations were characterized by multiple-particle tracking technology. This method allows simultaneous measurement of trajectories for hundreds of individual particles, facilitating relatively high throughput measurements[30]. Poly(ethylene oxide) (PEO) hydrogels was used as the diffusion medium[31]. The FITC-labeled liposomes (drug free) were first diluted 400-fold in the media, and then one drop was placed on a slide for observation with a fluorescence inverted microscope (DMI 4000B, Leica, Germany). Ten second movies (frame rate: 37 fps) were captured at a temporal resolution of 32.6 ms using LAS 4.5 software (Leica). The tracking process of the nanoparticles was analyzed using ImageJ software (NIH, Bethesda, MA, USA)[32]. Three independent measurements were conducted for each sample and 100 particles were analyzed in each test. The accumulative mean square displacement (MSD) and effective diffusivities ($D_{eff}$) were calculated using Eqs. (5) and (6), respectively:

$$MSD = [x(t + \tau) \; x(t)]^2 + [y(t + \tau) \; y(t)]^2 \qquad (5)$$

$$D_{eff} = MSD/(4\tau) \qquad (6)$$

where $x$ and $y$ are the coordinates of the liposomes in PEO hydrogels and $\tau$ is the time scale[33,34].

## 2.6. Cell cultures and animals

The human pancreatic stellate cell line HPaSteC was obtained from ScienCell Research Laboratories and cultured in DMEM, while the human pancreatic cancer cell line BxPC-3 was provided by the Cell Bank of the Chinese Academy of Sciences (Shanghai, China) in RPMI 1640 medium. All culture medium contained 10% FBS and 1% penicillin–streptomycin. Both cell lines were cultured at 37 °C in a 95% humidified atmosphere containing 5% $CO_2$.

Male BALB/c nude mice (20 ± 2 g), supplied by Shanghai Sippr-BK Laboratory Animal Co., Ltd. (Shanghai, China), were acclimatized at 25 °C and 55% humidity under natural light/dark conditions. All animal experiments were carried out under the guidelines approved by the Institutional Animal Care and Use Committee of Shanghai Institute of Materia Medica, Chinese Academy of Sciences.

## 2.7. Cellular uptake studies

The cellular uptake of the different liposomal preparations was measured using fluorescence microscopy and flow cytometry. Briefly, BxPC-3 and HPaSteC cells were seeded at a density of $3 \times 10^4$ cells/well in 24-well plates and incubated overnight to allow for attachment. Then, cells were incubated with different FITC-labeled liposomes at 37 °C for 2 h. The cells were washed with PBS three times, fixed with 4% paraformaldehyde for 10 min, and then stained with DAPI (10 µg/mL, 5 min). After washing in triplicate again, the cells were observed under a confocal laser scanning microscope (CLSM, FV1000, Olympus, Japan).

Quantitative analysis of the cellular uptake of the different liposomes was measured by flow cytometry. BxPC-3 and HPaSteC cells were seeded at a density of $5 \times 10^5$ cells/well in 24-well plates and incubated overnight to allow for attachment. Then, the cells were incubated with different FITC-labeled liposomes at 37 °C for 2 h. After washing in triplicate with cold PBS, the cells were trypsinized, collected, and analyzed using a flow cytometer (Becton Dickinson, USA).

## 2.8. In vitro cytotoxicity assay

The cytotoxicity of the drug-loaded liposomes in BxPC-3 and HPaSteC cells was evaluated using the MTT assay. In brief, BxPC-3 cells were seeded in 96-well plates at a density of 3000 cells/well in RPMI 1640 supplement for 24 h, while HPaSteC cells were seeded at 5000 cells/well in DMEM. Subsequently, the medium was replaced with different drug-loaded liposomes at DOX concentrations of 0.01, 0.05, 0.25, 1, 4, or 10 µg/mL for 24 h. The in vitro cytotoxicity assay was performed using the MTT method.

## 2.9. In vitro penetration and growth inhibition of tumor spheroids

To adequately demonstrate differences in tumor penetration, 3D tumor spheroids consisting of BxPC-3&HPaSteC cells were generated to simulate the complicated in vivo barrier that exists in tumors and hinders drug delivery[35,36]. These 3D tumor spheroids were cultured using a method described in previous studies[36]. Briefly, each well of a 48-well plate was charged with 150 µL of a sterile agarose solution (2%, w/v) and the plate was cooled to room temperature. BxPC-3 and HPaSteC cells in a quantity ratio of 1:1 were seeded into each well at a density of $1 \times 10^4$ cells/well. Then, the culture plates were agitated gently for 5 min and incubated at 37 °C for 4 days to allow for the spheroids to develop. Meanwhile, 3D tumor spheroids containing only BxPC-3 cells were also prepared.

The 3D tumor spheroids were cultured at 37 °C until reaching a uniform diameter of 300–400 µm. Then, they were incubated with FITC-labeled liposomes at 37 °C for 2 h. The tumor spheroids were washed in triplicate using PBS and fixed with 4% paraformaldehyde for 30 min. The permeation of the FITC-labeled liposomes within the spheroids was observed using a CLSM.

BxPC-3&HPaSteC tumor spheroids were used to measure growth inhibition by the various liposomal preparations. After the tumor spheroid diameters reached 320–340 µm, they were then incubated
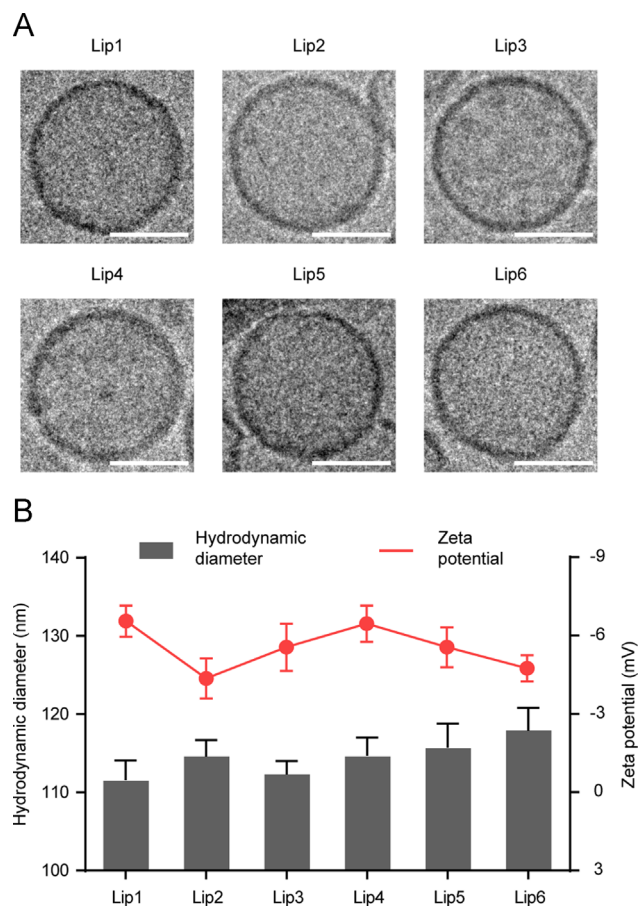


**Figure 1** Characterization of different liposomes. (A) Cryo-TEM images of different liposomes. Scale bar: 50 nm. (B) Hydrodynamic diameters and zeta potentials of liposomes determined via dynamic light scattering experiments. Data are presented as the mean ± SD ($n = 3$).

with 500 μLof culture media containing different liposomes with a DOX concentration of 0.5 μg/mL. Spheroids co-cultured with drug-free media served as controls. The maximum diameter (a) and minimum diameter (b) were characterized using an inverted fluorescence microscope (DMI 4000B, Leica, Germany) every 2 days (days 0, 2, 4, and 6), and the spheroid volume ($V$) was calculated using the following formula: $V = (ab^2)/2$. The change curve (%) of the volume was plotted to analyze and evaluate the tumor inhibitory effects of the various liposomes.

### 2.10. In vivo tumor penetration

BxPC-3&HPaSteC tumor-bearing nude mice were used for evaluating the in vivo tumor penetration. The nude mice were randomly divided into five groups after the tumors were ready ($n = 3$). FITC-labeled liposomes were injected peri-tumorally to the nude mice. At 4 h postinjection, the nude mice were sacrificed. The tumors were removed and washed by cold PBS in triplicate. Then, the tumors were sliced into 10 μm sections by a microtome cryostat (Leica CM1950, Germany). Finally, the tumor tissues were fixed by 4% paraformaldehyde and stained with DAPI, while tumor vessels were labeled by immunofluorescence staining with anti-CD31 antibody. After washing in triplicate, the tissues were observed under a CLSM.

### 2.11. In vivo anti-tumor effects

To evaluate the in vivo anti-tumor effects of the different preparations, BxPC-3&HPaSteC tumor-bearing nude mice were randomly divided into seven groups when the tumor volume reached approximately 70–90 mm[3]. The mice in the different groups were treated with various liposomal preparations five times at 3-day intervals (days 1, 4, 7, 10, and 13). All the preparations were injected peri-tumorally at an equivalent DOX dose of 1.6 mg/kg body weight. The mouse body weight and tumor volume ($V = w^2 \times l/2$, where $w$ and $l$ represent the width and length of the tumor as measured by caliper) were measured every 2 days. At the end of the experiment, one animal from each group was sacrificed and used for hematoxylin and eosin (H&E) staining and pathological study, while the remaining animals were monitored for two months to establish the survival rate.

### 2.12. Statistical analysis

Significant differences were evaluated using an independent-samples $t$-test and multiple treatment groups were compared within individual experiments by analysis of variance (ANOVA). $P$ values less than 0.05 were considered significant. Data are presented as the mean $\pm$ standard deviation (SD).

## 3. Results and discussions

### 3.1. Characterization of the liposomes

Particle size and size distribution significantly impact the development of suitable drug carriers for cancer therapeutics[9] as they influence the biodistribution, release and toxicity of the drug, as well as cellular uptake and tumor penetration. The characteristics of the different liposomes prepared in this study are summarized in Fig. 1. The hydrodynamic diameters of the prepared liposomes were found to be in a narrow range, from 112 to 118 nm. Furthermore, the polydispersity index (PDI) of the different preparations was also determined to be in a narrow range. These similar characteristics allowed for a more accurate comparison of the liposome preparations in terms of their ability to penetrate tumors and anti-tumor effects. The Cryo-TEM images showed that the liposomes were similar in size, and the images demonstrated no significant differences in morphology among the different liposomal preparations (Fig. 1A). As shown in Table 2, the actual contents of the liposomes slightly decreased because there was a little residue in the extruder, while the compositions of the preparations were consistent with the feeding ratio (Table 3). Liposomal rigidity was characterized by AFM, which showed that the liposomal membrane rigidity decreased when the cholesterol content was increased. This may be because that the liposomal membrane changed from a solid phase to a solid–liquid coexisting phase, and further to the liquid phase as the cholesterol increased. During this process, the rigidity of the liposomal membrane was continuously reduced[26,28].

The EE% of all the preparations was found to be greater than 90% (Table 1), which was attributed to the ammonium sulfate gradient. Our data suggested that the slightly higher entrapment efficiency of DOX from Lip2 to Lip5 might be due to the addition of cholesterol, which enhanced the liposomal stability[37]. However,

**Table 3**  The actual contents and compositions of components in the liposomes.

| Preparations | Composition (molar ratio) | Composition (mass ratio) |
|---|---|---|
| Lip1 | 97.5:/:2.5 | 4.88:/:0.44 |
| Lip2 | 77.6:19.9:2.5 | 4.27:0.54:0.49 |
| Lip3 | 67.3:30.1:2.6 | 3.92:0.86:0.52 |
| Lip4 | 57.7:39.8:2.5 | 3.57:1.22:0.55 |
| Lip5 | 47.7:49.8:2.5 | 3.11:1.60:0.59 |
| Lip6 | 56.5:38.2:5.3 | 3.20:1.06:1.05 |

Compositions of preparations are shown as HSPC:cholesterol: DSPE-PEG$_{2000}$.
/, not applicable.

**Table 2**  Recovery ratio (%) of different compositions in liposomes.

| Composition | Recovery ratio (%) | | | | | |
|---|---|---|---|---|---|---|
|  | Lip1 | Lip2 | Lip3 | Lip4 | Lip5 | Lip6 |
| HSPC | 98.6 $\pm$ 1.4 | 98.1 $\pm$ 2.0 | 98.0 $\pm$ 1.6 | 99.2 $\pm$ 1.9 | 98.2 $\pm$ 1.5 | 98.9 $\pm$ 1.7 |
| Cholesterol | / | 97.5 $\pm$ 1.7 | 98.8 $\pm$ 2.3 | 98.4 $\pm$ 2.0 | 97.5 $\pm$ 1.4 | 98.0 $\pm$ 2.2 |
| DSPE-PEG$_{2000}$ | 98.1 $\pm$ 1.8 | 98.1 $\pm$ 2.1 | 97.7 $\pm$ 1.7 | 98.5 $\pm$ 1.5 | 97.9 $\pm$ 2.1 | 97.3 $\pm$ 2.4 |

Data are presented as the mean $\pm$ SD ($n = 3$).
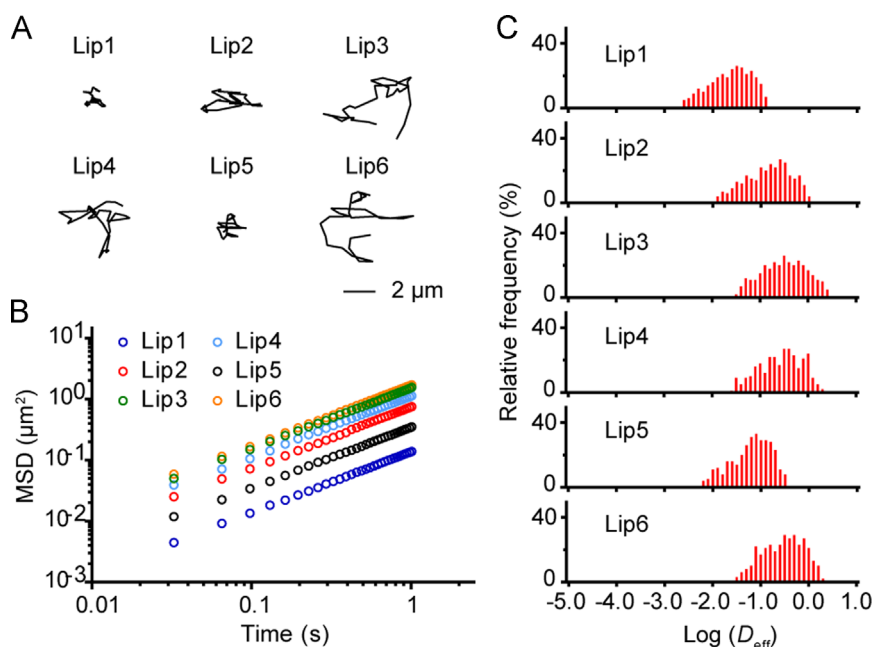/, not applicable.

**Figure 2** Multiple-particle tracking of different preparations. (A) Representative trajectories for the different liposomal preparations in PEO hydrogels on a time scale of 1 s. (B) Ensemble-averaged geometric mean square displacement (MSD) as a function of time over 1 s. (C) Distributions of the logarithms of individual particle effective diffusivities ($D_{eff}$) on a time scale of 1 s. The data represents three independent experiments, and each experiment tracked 100 NPs.

no significant differences in DOX encapsulation were observed among the preparations (Lip2 to Lip5).

## 3.2. In vitro drug release

Drug release studies were performed using the dialysis method in PBS at pH 7.4. As shown in Supporting Information Fig. S1, all the preparations were found to give slow and sustained drug release. As the cholesterol content increased, the liposomal cumulative release rate decreased, with Lip1 providing the highest drug release rate and Lip5 giving the lowest drug release rate. During the 100 h accumulative drug release study, only 30% of the DOX was released from Lip5. This outcome might be due to the high cholesterol content causing an increase in the order of the lipid membrane and consequently preventing the leakage of DOX from the preparation[21]. The in vitro drug release profiles suggested that the drug-loaded liposomes might retain most of the encapsulated drug during the penetration process.

## 3.3. Multiple-particle tracking

Multiple-particle tracking technology provides a rapid, nondestructive and highly sensitive method to detect particle behavior in a complex biological milieu[33]. We used this method to assess the diffusion of different liposomes in PEO hydrogels[31]. PEO hydrogels has been proven to form a stable fibrous structure[38] and disperses the required optical probes evenly[39]. Recently, it has been used to study the diffusion processes of nanoparticles[34]. The representative trajectories of different liposomes are mapped in Fig. 2A. It was observed that Lip1 moved within a small area, indicating that Lip1 was nearly trapped in the media. In contrast, liposomes were able to move more freely in a large area with the addition of cholesterol and were not hindered by the grid constructed from PEO hydrogels. However, as the proportion of cholesterol was increased further, the diffusion process was found to be

significantly limited as demonstrated by Lip5. These results reflected the relationship between liposomal rigidity and diffusibility, suggesting that liposomes with moderate rigidity diffuse more rapidly. To prove the significance of this conclusion, a preparation of Doxil® (Lip6) was tested which has been proven to be an effect preparation in anti-tumor therapeutics[40]. Lip6 is characterized as being at a higher PEGylation level, which has been shown to have a pronounced effect on enhancing diffusion[41,42]. Importantly, the enhancement elicited by fine adjustment of the cholesterol content (between Lip3 and Lip4) was comparable with that observed with multiple PEGylation (Lip4–Lip6). Next, MSD, a quantitative measurement of diffusion, was calculated on the time scale of 1 s (Fig. 2B). The MSD of Lip3 was found to be approximately 11.1-fold and 4.4-fold higher than that of Lip1 and Lip5, respectively. To make sure that the observed rapid transportation of liposomes was not biased by a small fraction of rapid-diffusion outlier liposomes, the distribution of effective diffusivities ($D_{eff}$) was further examined. After examination of the distribution of effective diffusivities, we confirmed that the selected particles were representative of the particle population (Fig. 2C). Given the above findings, it was concluded that liposomes with moderate membrane rigidity consistently exhibited higher diffusivities, and that increased diffusion rates might represent deeper tumor penetration.

## 3.4. Cellular uptake

The cellular uptake of liposomes in BxPC-3 and HPaSteC cells was evaluated by a CLSM and flow cytometry. As shown in Fig. 3A, BxPC-3 and HPaSteC cells incubated with FITC-labeled Lip1 exhibited strong green fluorescence, indicating excellent cellular uptake. Lip2 and Lip3 displayed moderate fluorescence, while Lip4 and Lip5 showed reduced fluorescence. In addition, the cellular uptake of different liposomes was investigated quantitatively by flow cytometry (Fig. 3B and C). From these experiments, it was obvious that the cellular uptake decreased when the liposomal cholesterol
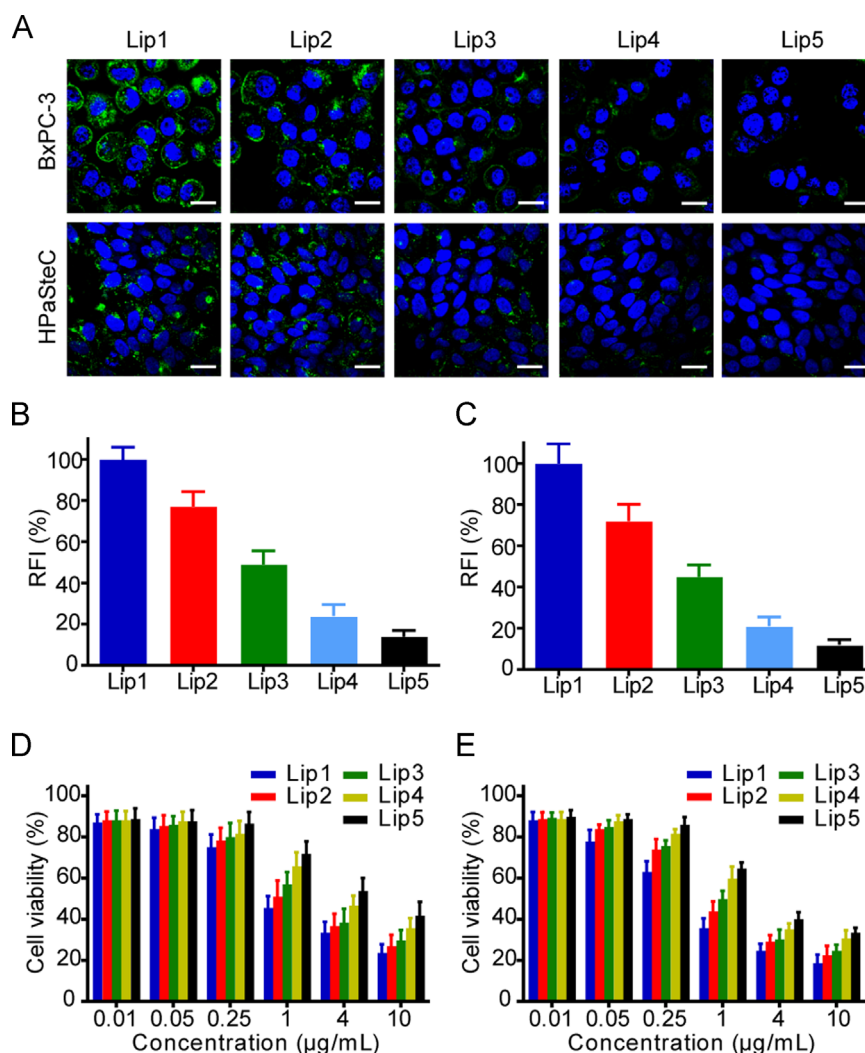
**Figure 3** Cellular uptake of FITC-labeled liposomes and cytotoxicity of drug-loaded liposomes. (A) Cellular uptake of FITC-labeled liposomes in BxPC-3 and HPaSteC cells. (B) and (C) Mean fluorescence intensity (MFI) quantification of BxPC-3 and HPaSteC cells, respectively. Data are presented as the mean $\pm$ SD ($n$ = 3). Scale bar: 50 μm. (D) Cytotoxicity study of the different liposomes in BxPC-3 cells ($n$ = 6). (E) Cytotoxicity study of the different liposomes in HPaSteC cells. Data are presented as the mean $\pm$ SD ($n$ = 6).

**Table 4** $IC_{50}$ values of different liposomes in BxPC-3 and HPaSteC cells.

| Cell | $IC_{50}$ of liposomes (μg/mL) | | | | |
|---|---|---|---|---|---|
| | Lip1 | Lip2 | Lip3 | Lip4 | Lip5 |
| BxPC-3 | $0.74 \pm 0.26$ | $0.90 \pm 0.31$ | $1.16 \pm 0.26$ | $1.78 \pm 0.36$ | $2.51 \pm 0.55$ |
| HPaSteC | $0.40 \pm 0.18$ | $0.66 \pm 0.23$ | $0.83 \pm 0.25$ | $1.26 \pm 0.33$ | $1.63 \pm 0.48$ |

Data are presented as the mean $\pm$ SD ($n$ = 3).

content increased. For example, significant differences in the cellular uptake were observed when the proportion of cholesterol reached 40% and 50%. Moreover, the changes in cellular uptake were similar to the Young's modulus with the addition of cholesterol (Table 1). Therefore, we hypothesized that as the cholesterol content was increased, the membrane rigidity of the liposomal preparations was decreased, resulting in the lower cellular uptake. This may be because liposomal membranes with less rigidity increased the contact surface with the cells, resulting in prolonged uptake time[16]. Soft membranes

may also undergo significant deformation during the cellular uptake which consumed more energy[23].

### 3.5. In vitro cytotoxicity assay

The *in vitro* anti-tumor activity of the drug-loaded liposomes was evaluated *via* the MTT assay using BxPC-3 and HPaSteC cells. The half maximal inhibitory concentration ($IC_{50}$) values of the different preparations are listed in Table 4. After 24 h incubation,

cytotoxicity was found to increase with increasing drug concentrations for all groups and decreased when cholesterol was added to the preparations (Fig. 3D and E). It is well known that DOX exerts its effect in the nucleus[43]. Therefore, to get the effective anti-tumor efficacy, the liposomes must be taken up by cells and then release DOX inside the cell[44]. From the above results, we concluded that cytotoxicity was mainly affected by cellular uptake (cytotoxicity increased with increased cellular uptake) and was supplemented by drug release.

## 3.6. In vitro penetration and growth inhibition of tumor spheroids

As one of the most recalcitrant human tumors, pancreatic ductal adenocarcinoma (PDA) has an extremely dense stroma compared to other solid tumors[45]. The stroma acts as a stable physical barrier that impedes penetration by drug carriers, resulting in poor anti-tumor effects[4]. Recently, 3D tumor spheroids have been developed to simulate in vivo tumor tissue and have been used to effectively and conveniently characterize the tumor penetration properties of drug carriers[46–48]. In this study, 3D tumor spheroids were constructed from BxPC-3 and HPaSteC cells to mimic complex in vivo tumor barriers, such as the in vivo fibrotic barrier and the interaction between the pancreatic stellate cells and the tumor cells[49]. Spheroids containing only BxPC-3 cells were also prepared for comparison. The BxPC-3&HPaSteC co-cultured tumor spheroids were proven to be well-formed by previous research in our laboratory[36].

The penetration activities of FITC-labeled liposomes in the BxPC-3&HPaSteC co-cultured tumor spheroids were determined by a CLSM. After incubation with different preparations for 2 h, tumor penetration was measured by CLSM Z-stack scanning and the spheroid surface was defined as 0 μm. As shown in Fig. 4A, liposomal tumor penetration represented by fluorescence intensity was in the following order: Lip3 > Lip2 > Lip4 > Lip1 > Lip5. Differences in tumor penetration between liposomal preparations are shown more vividly and intuitively in Fig. 4C and E. These results were slightly different from those of multiple-particle tracking (Table 1) and this discrepancy likely resulted from the liposomes not being ingested by the multiple-particle tracking medium. In these tumor spheroids, the dual barriers of drug delivery (tumor penetration and cellular uptake) could be examined. The liposomes with moderate membrane rigidity could overcome the fibrotic structure to penetrate deeply into the spheroids and then they can be ingested by the internal cells efficiently. However, the liposomes with lower and higher rigidity might be trapped in the surface of the tumor spheroids. Taken together with the results from multiple-particle tracking and cellular, we could better understand the above results using tumor spheroids. The green fluorescence of Lip3 and Lip2 was clearly observed even at a scanning depth of 50 μm. This notable fluorescence might result from a synergistic effect between the relatively good tumor penetration and cellular uptake of these liposomal preparations. In contrast, Lip1 could only be taken up by superficial cells of the tumor spheroids due to poor tumor penetration, despite having the strongest cellular uptake. Meanwhile, the weaker fluorescence intensity of Lip4 might result from its relatively poor cellular uptake. Because the penetration process in tumor spheroids is dynamic, preparations that are not quickly taken up may be pushed out of the tumor by the tumor microenvironment[3].

Tumor spheroid penetration resulted from spheroids generated with BxPC-3 cells only are shown in Fig. 4B, D and F, and the results showed a similar trend as those from the cellular uptake studies. These results might be interpreted as the liposomes having readily penetrated the tumor spheroids, which lack a dense stroma. To some extent, function of tumor penetration in drug delivery was reduced. The results were close to the 2D monolayer cellular uptake. This experiment indirectly proved that tumor penetration and cellular uptake were both responsible for the results in the BxPC-3&HPaSteC co-cultured tumor spheroid study. Comparing the data from the two spheroid models, one could conclude that for a complex and recalcitrant tumor, such as PDA, tumor penetration plays a decisive role because the dense stroma traps most of the inactive liposomes on the tumor tissue surface. Clearly, the choice of 3D tumor spheroids generated from BxPC-3&HPaSteC cells was critical to the success of these experiments.

Next, we used the BxPC-3&HPaSteC co-cultured tumor spheroids to study tumor spheroid growth inhibition. The tumor spheroids treated with different preparations were imaged on days 0, 2, 4 and 6 (Fig. 5A), and spheroid growth curves were generated (Fig. 5B). Lip3 and Lip2, with moderate membrane rigidity, significantly inhibited the growth of the tumor spheroids and provided superior growth inhibition than the commercial preparation of Doxil® (Lip6). The inhibition rates of Lip1 and Lip5 were lower, which was expected given the conclusions that were drawn from the previous tumor spheroid penetration experiments described above.

## 3.7. In vivo tumor penetration

To verify the tumor penetration ability of the liposomes more vividly, the in vivo tumor penetration experiment was examined. After the incubation with different preparations, tumor tissue slices were prepared and observed by a CLSM. As shown in Fig. 6, Lip2 and Lip3 with bright and widespread fluorescence indicated excellent tumor penetration. Whereas, the partial high fluorescence intensity of Lip1 was not occurred. This might because tissue slices are not in direct contact with the preparations compared to the tumor spheroids. The cellular uptake superiority of Lip1 did not act until Lip1 arrived at the slice depth. For Lip4, its cellular uptake ability may put itself at a disadvantage in resisting body clearance, resulting in lower fluorescence intensity compared to Lip2 and Lip3. These results were consistent with those of the in vitro tumor spheroid penetration.

## 3.8. In vivo anti-tumor effects

To further verify the in vivo anti-tumor effects of the liposomal preparations, BxPC3&HPaSteC tumor-bearing nude mice were treated with different liposomal preparations by peri-tumoral injection after the tumor volume reached 70–90 mm³. As indicated in Fig. 7A and C, the Lip1 and Lip5 treatment groups showed slight tumor inhibition compared to the saline group. The modest tumor growth inhibition could be attributed to poor tumor penetration, which resulted in low drug availability, despite Lip1 having the best cellular uptake among the preparations. Lip4 showed improved tumor growth inhibition, which was aroused from increased tumor penetration. As expected, Lip2 and Lip3 exhibited excellent tumor growth inhibition. These results were consistent with the growth inhibitory effects observed in the in vitro tumor spheroid studies (Fig. 5B). The addition of an
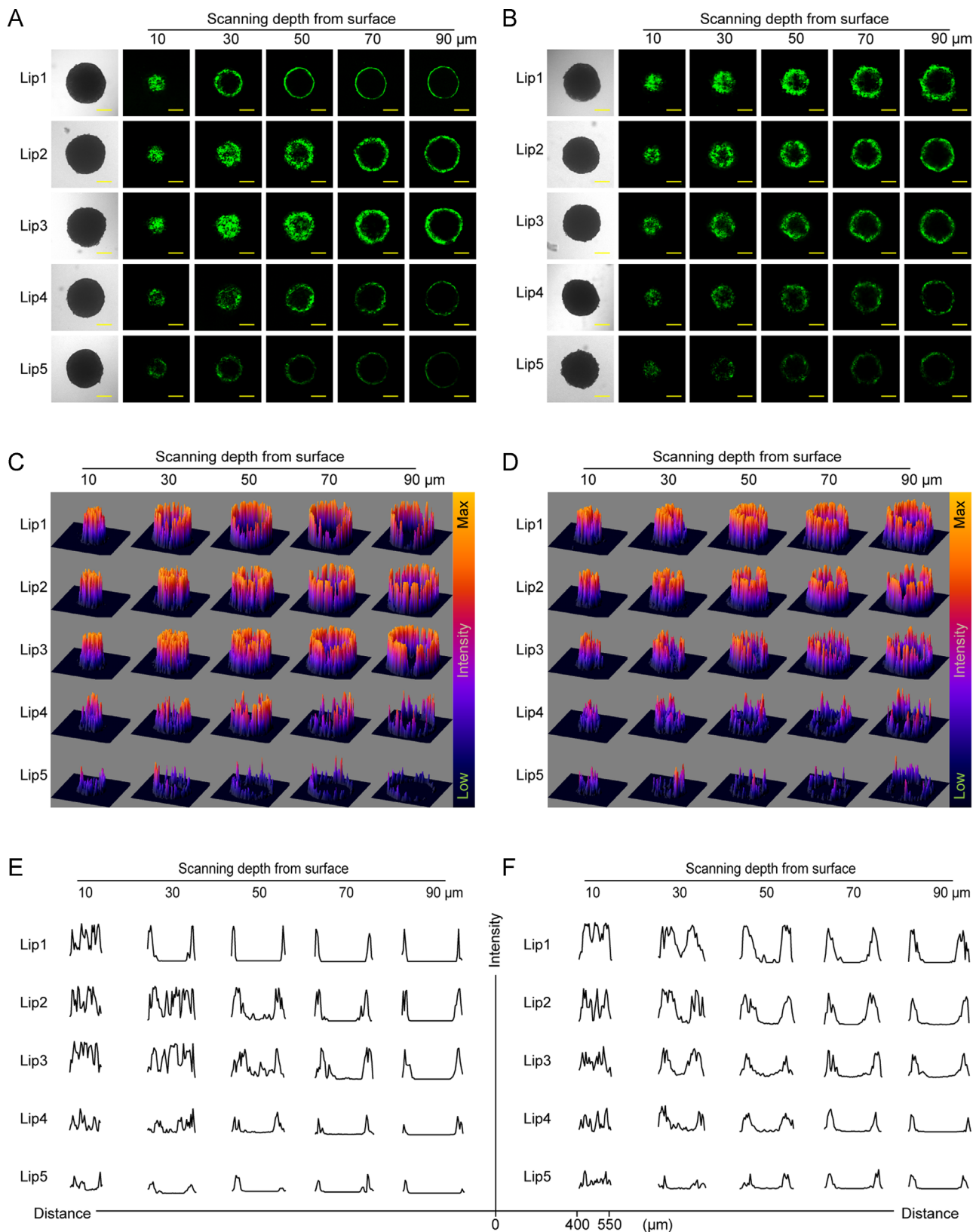
**Figure 4** *In vitro* penetration of tumor spheroids. (A) and (B) Z-Stack fluorescence images of BxPC-3&HPaSteC and BxPC-3 spheroids after incubation with various FITC-labeled liposomes for 2 h, respectively. (C) and (D) 3D-Renderings of BxPC-3&HPaSteC and BxPC-3 spheroid penetration, respectively. (E) and (F) Fluorescence distribution along the narrow region within BxPC-3&HPaSteC and BxPC-3 spheroids, respectively. Scale bar: 150 μm.
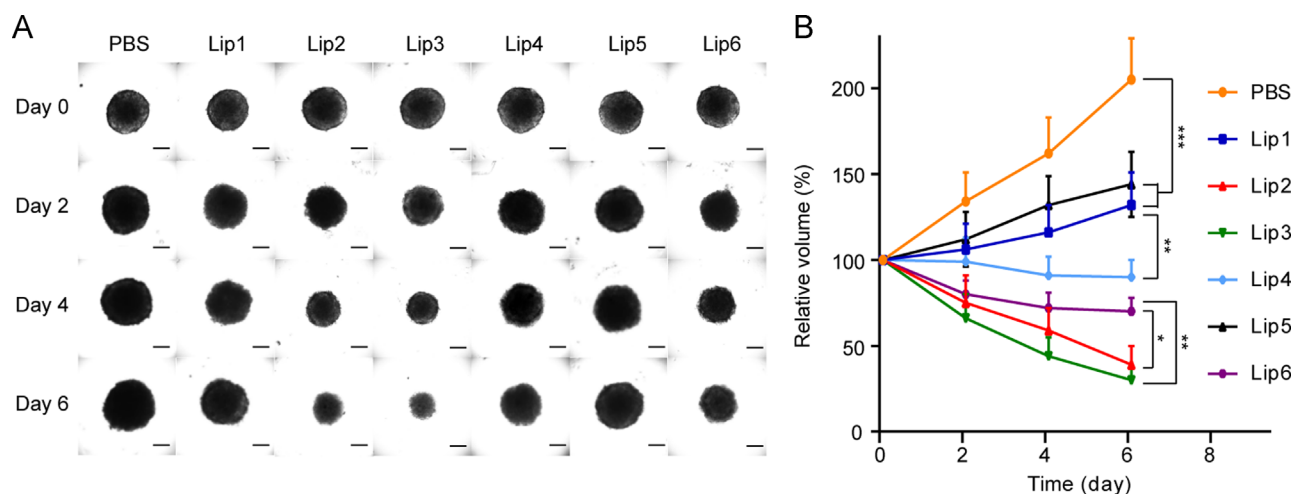
**Figure 5** *In vitro* growth inhibition of tumor spheroids. (A) Representative images of BxPC-3&HPaSteC spheroids observed using an inverted fluorescence microscope after treatment with different drug-loaded liposomes. DOX concentrations were 0.5 μg/mL. (B) The corresponding tumor spheroid growth curves of BxPC-3&HPaSteC spheroids treated with different drug-loaded liposomes. Data are presented as the mean $\pm$ SD ($n = 5$). $^{*}P < 0.05$, $^{**}P < 0.01$, and $^{***}P < 0.001$. Scale bar: 150 μm.
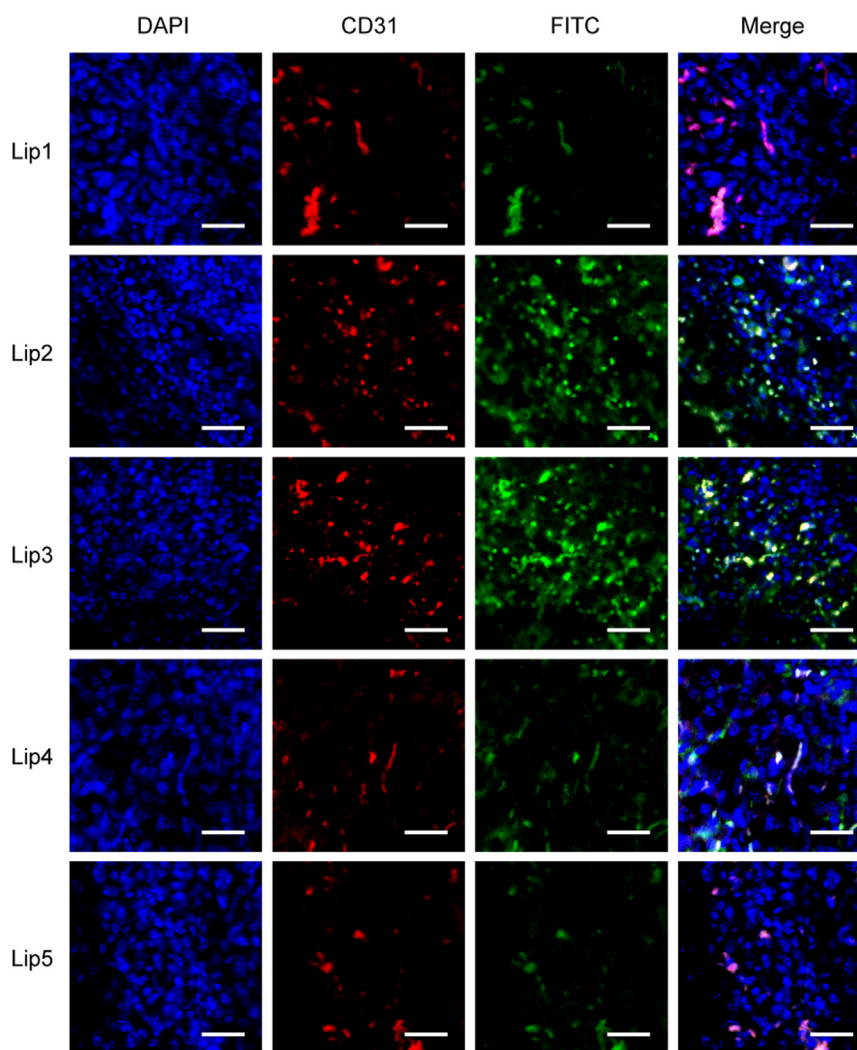


**Figure 6** *In vivo* tumor penetration. FITC-labeled liposomes were used in the experiment. Cell nuclei and tumor vessels were stained with DAPI and anti-CD31 antibody, respectively. Scale bar: 20 μm.
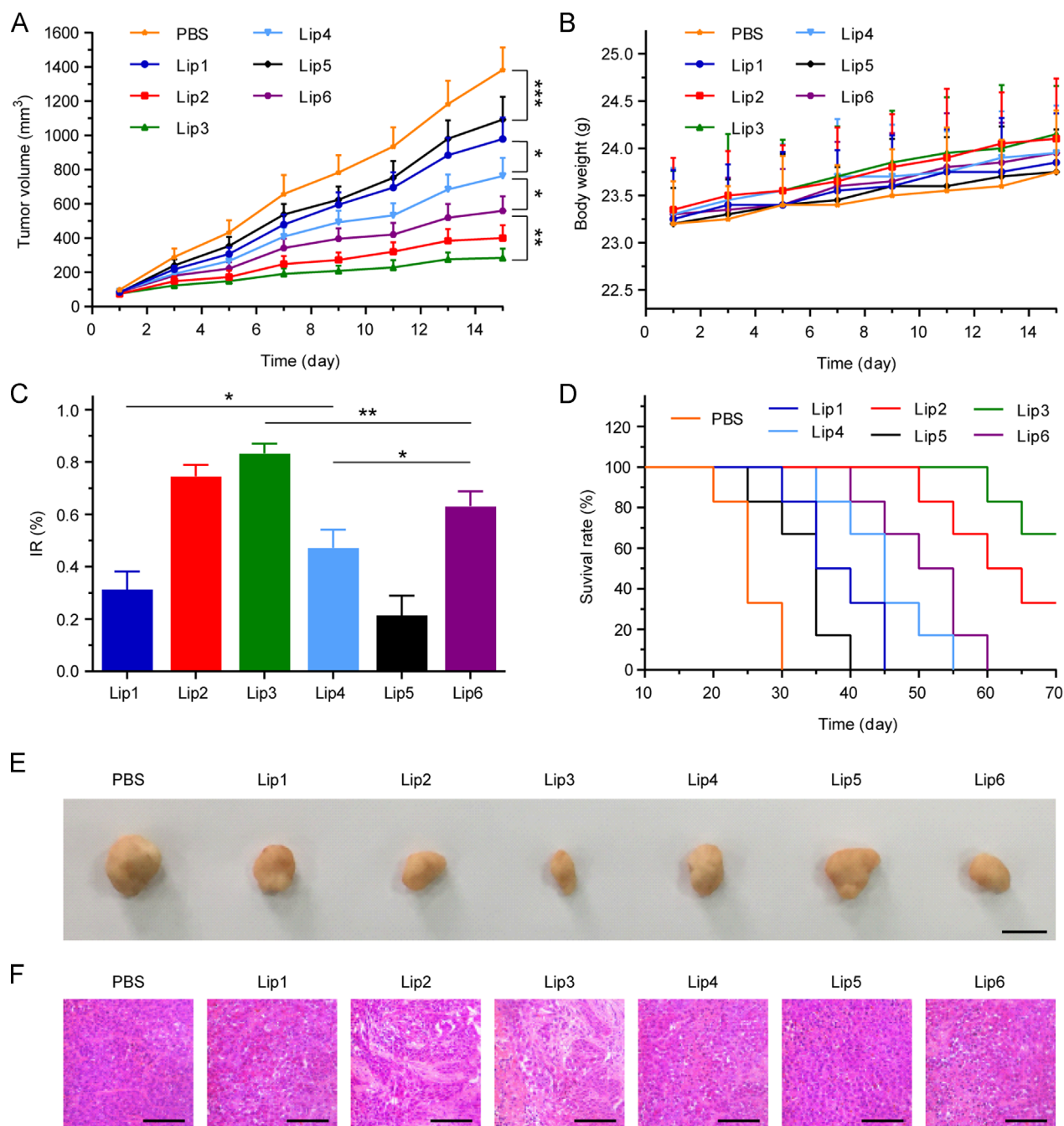
**Figure 7** *In vivo* anti-tumor effects. Nude mice bearing BxPC-3&HPaSteC tumors were treated with the indicated preparations for two weeks. These treatments were injected five times (days 1, 4, 7, 10, and 13) peri-tumorally with equivalent DOX doses of 1.6 mg/kg. (A) Tumor growth curve during the whole experiment. (B) The body weight changes of BxPC-3&HPaSteC-bearing nude mice during treatment. (C) Tumor inhibition rate. (D) Survival curve. (E) Representative tumor xenograft images. Scale bar: 10 mm. (F) Images of H&E-stained tumor slices excised from subcutaneous tumor-bearing mice. Data are presented as the mean $\pm$ SD ($n = 6$). $^{*}P < 0.05$, $^{**}P < 0.01$, and $^{***}P < 0.001$. Scale bar: 100 μm.

appropriate amount of cholesterol enhanced the liposomal tumor penetration significantly while maintaining a certain level of cellular uptake, thereby enhancing the anti-tumor effect. As is well known, only when liposomes penetrate deeply into the tumor tissues can they be taken up by the internal tumor cells to give an effective therapeutic response[50]. In this study, considering the characteristics of the preparations, we speculated that the significant differences observed in tumor penetration and anti-tumor effects could be attributed to the changes in the liposomal

membrane rigidity, which was in turn affected by the cholesterol content. At the end of treatment, tumor xenografts were excised and imaged from representative animals in each treatment group (Fig. 7E), while the remaining animals were monitored to determine the survival rate.

The body weights of the nude mice were measured to investigate the *in vivo* systemic toxicity of the preparations[51]. In this study, the liposomal preparations were stable (Supporting Information Fig. S1) and were administered by peri-tumoral

injection, leading to low systemic toxicity. Therefore, we concluded that the differences in body weight mainly depended on the anti-tumor effects, because tumors with high growth inhibition consume less nutrition than those with low tumor growth inhibition. As shown in Fig. 7B, in all the groups, the body weights of the nude mice showed a slight increase relative to the initial body weight on day 1. The groups with optimal cholesterol and moderate membrane rigidity displayed more weight gain compared to the other groups, indicating better therapeutic effects.

After observing the tumor growth trends during the first 14 days after dosing, survival rates were investigated using Kaplan-Meier survival curve analysis. As shown in Fig. 7D, survival rates were consistent with the results from the tumor growth inhibition study. Furthermore, *ex vivo* assays of the tumors were performed to observe the behavior of the cancerous cells after treatment with the different liposomal preparations. Tumor sections were harvested from the different groups for histological analysis by H&E staining (Fig. 7F). Liposomes with moderate membrane rigidity displayed a lower density of available cells due to their superior anti-tumor effects.

In this study, liposomal membrane rigidity decreased with the cholesterol content increased, leading to decreasing cellular uptake. The liposomes with moderate membrane rigidity gained better diffusivity compared to those with lower or higher rigidity, which enabled them to overcome the fibrotic structure to penetrate deeply into the spheroids. However, the liposomes with lower or higher rigidity might be trapped in the surface of the tumor spheroids. In the anti-tumor efficacy studies, the moderate rigid liposomes have also displayed their superiority in the therapeutic of tumors with dense stroma.

## 4. Conclusions

In this study, we prepared liposomes with different cholesterol content to explore the influence of liposomal membrane rigidity on tumor penetration and anti-tumor effects. AFM experiments proved that liposomal rigidity decreased with the addition of cholesterol. Diffusion properties were determined using multiple-particle tracking technology and the results showed that liposomes with moderate membrane rigidity diffused more rapidly in PEO hydrogels. BxPC-3&HPaSteC co-cultured tumor spheroids and BxPC-3&HPaSteC tumor-bearing nude mice were constructed to explore the tumor penetration and anti-tumor effects of the liposomal preparations. The results indicated that a certain cholesterol content clearly improved the tumor penetration and anti-tumor effects of the liposomal preparations, and we concluded that these phenomena were due to changes in the liposomal membrane rigidity. The present study not only reveals the relationship between liposomal membrane rigidity and tumor penetration but also provides an effective and convenient method to enhance the tumor penetration and anti-tumor effects of liposomes by changing the cholesterol content.

## Appendix A. Supporting information

Supporting data associated with this article can be found in the online version at https://doi.org/10.1016/j.apsb.2019.02.010.

## References

1. Li HJ, Du JZ, Liu J, Du XJ, Shen S, Zhu YH, et al. Smart superstructures with ultrahigh pH-sensitivity for targeting acidic tumor microenvironment: instantaneous size switching and improved tumor penetration. *ACS Nano* 2016;**10**:6753–61.
2. Li HJ, Du JZ, Du XJ, Xu CF, Sun CY, Wang HX, et al. Stimuli-responsive clustered nanoparticles for improved tumor penetration and therapeutic efficacy. *Proc Natl Acad Sci U S A* 2016;**113**:4164–9.
3. Sun QH, Zhou ZX, Qiu NS, Shen YQ. Rational design of cancer nanomedicine: nanoproperty integration and synchronization. *Adv Mater* 2017;**29**:1606628.
4. Kaur S, Kumar S, Momi N, Sasson AR, Batra SK. Mucins in pancreatic cancer and its microenvironment. *Nat Rev Gastroenterol Hepatol* 2013;**10**:607–20.
5. Bhaw-Luximon A, Jhurry D. New avenues for improving pancreatic ductal adenocarcinoma (PDAC) treatment: selective stroma depletion combined with nano drug delivery. *Cancer Lett* 2015;**369**:266–73.
6. Curry FR. Drug delivery: redefining tumour vascular barriers. *Nat Nanotechnol* 2016;**11**:494–6.
7. Levental KR, Yu H, Kass L, Lakins JN, Egeblad M, Erler JT, et al. Matrix crosslinking forces tumor progression by enhancing integrin signaling. *Cell* 2009;**139**:891–906.
8. Daraee H, Etemadi A, Kouhi M, Alimirzalu S, Akbarzadeh A. Application of liposomes in medicine and drug delivery. *Artif Cells Nanomed Biotechnol* 2014;**44**:381–91.
9. Zhang J, Luo Y, Zhao X, Li X, Li K, Chen D, et al. Co-delivery of doxorubicin and the traditional Chinese medicine quercetin using biotin-PEG$_{2000}$-DSPE modified liposomes for the treatment of multi-drug resistant breast cancer. *RSC Adv* 2016;**6**:113173–84.
10. Hong EJ, Choi DG, Shim MS. Targeted and effective photodynamic therapy for cancer using functionalized nanomaterials. *Acta Pharm Sin B* 2016;**6**:297–307.
11. Cabral H, Matsumoto Y, Mizuno K, Chen Q, Murakami M, Kimura M, et al. Accumulation of sub-100 nm polymeric micelles in poorly permeable tumours depends on size. *Nat Nanotechnol* 2011;**6**:815–23.
12. Wang HX, Zuo ZQ, Du JZ, Wang YC, Sun R, Cao ZT,, et al. Surface charge critically affects tumor penetration and therapeutic efficacy of cancer nanomedicines. *Nano Today* 2016;**11**:133–44.
13. Taha EI, Elanazi MH, Elbagory IM, Bayomi MA. Design of liposomal colloidal systems for ocular delivery of ciprofloxacin. *Saudi Pharm J* 2014;**22**:231–9.
14. Roy B, Guha P, Bhattarai R, Nahak P, Karmakar G, Chettri P, et al. Influence of lipid composition, pH, and temperature on physicochemical properties of liposomes with curcumin as model drug. *J Oleo Sci* 2016;**65**:399–411.
15. Guo P, Liu D, Subramanyam K, Wang B, Yang J, Huang J, et al. Nanoparticle elasticity directs tumor uptake. *Nat Commun* 2018;**9**:130.
16. Stern T, Kaner I, Laser Zer N, Shoval H, Dror D, Manevitch Z, et al. Rigidity of polymer micelles affects interactions with tumor cells. *J Control Release* 2017;**257**:40–50.
17. Nakano K, Tozuka Y, Yamamoto H, Kawashima Y, Takeuchi H. A novel method for measuring rigidity of submicron-size liposomes with atomic force microscopy. *Int J Pharm* 2008;**355**:203–9.
18. Spyratou E, Mourelatou EA, Makropoulou M, Demetzos C. Atomic force microscopy: a tool to study the structure, dynamics and stability of liposomal drug delivery systems. *Expert Opin Drug Deliv* 2009;**6**:305–17.
19. Deng H, Song K, Zhang J, Deng L, Dong A, Qin Z. Modulating the rigidity of nanoparticles for tumor penetration. *Chem Commun* 2018;**54**:3014–7.

20. Rog T, Pasenkiewicz-Gierula M, Vattulainen I, Karttunen M. Ordering effects of cholesterol and its analogues. *Biochim Biophys Acta* 2009;**1788**:97–121.

21. Sadeghi N, Deckers R, Ozbakir B, Akthar S, Kok RJ, Lammers T, et al. Influence of cholesterol inclusion on the doxorubicin release characteristics of lysolipid-based thermosensitive liposomes. *Int J Pharm* 2018;**548**:778–82.

22. Khelashvili G, Johner N, Zhao G, Harries D, Scott HL. Molecular origins of bending rigidity in lipids with isolated and conjugated double bonds: the effect of cholesterol. *Chem Phys Lipids* 2014;**178**:18–26.

23. Sun J, Zhang L, Wang J, Feng Q, Liu D, Yin Q, et al. Tunable rigidity of (polymeric core)-(lipid shell) nanoparticles for regulated cellular uptake. *Adv Mater* 2015;**27**:1402–7.

24. Song J, Waugh RE. Bending rigidity of SOPC membranes containing cholesterol. *Biophys J* 1993;**64**:1967–70.

25. Tristramnagle S. Structure and bending rigidity of fully hydrated lipid bilayers with added peptides and cholesterol using diffuse X-ray scattering. *Biophys J* 2009;**96** [1a-1a] .

26. Gracià RS, Bezlyepkina N, Knorr RL, Lipowsky R, Dimova R. Effect of cholesterol on the rigidity of saturated and unsaturated membranes: fluctuation and electrodeformation analysis of giant vesicles. *Soft Matter* 2010;**6**:1472–82.

27. An H, Nussio MR, Huson MG, Voelcker NH, Shapter JG. Material properties of lipid microdomains: force-volume imaging study of the effect of cholesterol on lipid microdomain rigidity. *Biophys J* 2010;**99**:834–44.

28. Takechi-Haraya Y, Sakai-Kato K, Abe Y, Kawanishi T, Okuda H, Goda Y. Atomic Force Microscopic Analysis of the Effect of Lipid Composition on Liposome Membrane Rigidity. *Langmuir* 2016;**32**:6074–82.

29. Shibata H, Yomota C, Okuda H. Simultaneous determination of polyethylene glycol-conjugated liposome components by using reversed-phase high-performance liquid chromatography with UV and evaporative light scattering detection. *AAPS PharmSciTech* 2013;**14**:811–7.

30. Wadajkar AS, Dancy JG, Roberts NB, Connolly NP, Strickland DK, Winkles JA, et al. Decreased non-specific adhesivity, receptor targeted (DART) nanoparticles exhibit improved dispersion, cellular uptake, and tumor retention in invasive gliomas. *J Control Release* 2017;**267**:144–53.

31. Chhetri RK, Blackmon RL, Wu WC, Hill DB, Button B, Casbas-Hernandez P, et al. Probing biological nanotopology *via* diffusion of weakly constrained plasmonic nanorods with optical coherence tomography. *Proc Natl Acad Sci U S A* 2014;**111**:E4289–97.

32. Meijering E, Dzyubachyk O, Smal I. Methods for cell and particle tracking. *Methods Enzymol* 2012;**504**:183–200.

33. Yu M, Wang J, Yang Y, Zhu C, Su Q, Guo S, et al. Rotation-facilitated rapid transport of nanorods in mucosal tissues. *Nano Lett* 2016;**16**:7176–82.

34. Yu M, Xu L, Tian F, Su Q, Zheng N, Yang Y, et al. Rapid transport of deformation-tuned nanoparticles across biological hydrogels and cellular barriers. *Nat Commun* 2018;**9**:2607.

35. Park JI, Lee J, Kwon JL, Park HB, Lee SY, Kim JY, et al. Scaffold-free coculture spheroids of human colonic adenocarcinoma cells and normal colonic fibroblasts promote tumorigenicity in nude mice. *Transl Oncol* 2016;**9**:79–88.

36. Wei Y, Wang Y, Xia D, Guo S, Wang F, Zhang X, et al. Thermosensitive liposomal codelivery of HSA–paclitaxel and HSA–ellagic acid complexes for enhanced drug perfusion and efficacy against pancreatic cancer. *ACS Appl Mater Interfaces* 2017;**9**:25138–51.

37. Redondo-Morata L, Giannotti MI, Sanz F. Influence of cholesterol on the phase transition of lipid bilayers: a temperature-controlled force spectroscopy study. *Langmuir* 2012;**28**(35)12851–60.

38. Schultz KM, Campo-Deano L, Baldwin AD, Kiick KL, Clasen C, Furst EM. Electrospinning covalently cross-linking biocompatible hydrogelators. *Polymer* 2013;**54**:363–71.

39. van Zanten JH, Amin S, Abdala AA. Brownian motion of colloidal spheres in aqueous PEO solutions. *Macromolecules* 2004;**37**:3874–80.

40. Barenholz Y. Doxil®—the first FDA-approved nano-drug: lessons learned. *J Control Release* 2012;**160**:117–34.

41. Shan W, Zhu X, Liu M, Li L, Zhong J, Sun W, et al. Overcoming the diffusion barrier of mucus and absorption barrier of epithelium by self-assembled nanoparticles for oral delivery of insulin. *ACS Nano* 2015;**9**:2345–56.

42. Lai SK, Wang YY, Hanes J. Mucus-penetrating nanoparticles for drug and gene delivery to mucosal tissues. *Adv Drug Deliv Rev* 2009;**61**:158–71.

43. Yang L, Wang Z, Wang J, Jiang W, Jiang X, Bai Z, et al. Doxorubicin conjugated functionalizable carbon dots for nucleus targeted delivery and enhanced therapeutic efficacy. *Nanoscale* 2016;**8**:6801–9.

44. Wennberg CL, van der Spoel D, Hub JS. Large influence of cholesterol on solute partitioning into lipid membranes. *J Am Chem Soc* 2012;**134**:5351–61.

45. Mahadevan D, Von Hoff DD. Tumor–stroma interactions in pancreatic ductal adenocarcinoma. *Mol Cancer Ther* 2007;**6**:1186–97.

46. Lu H, Stenzel MH. Multicellular tumor spheroids (MCTS) as a 3D *in vitro* evaluation tool of nanoparticles. *Small* 2018;**14**:e1702858.

47. Zhang M, Lu W. Enhanced glioma-targeting and stability of LGICP peptide coupled with stabilized peptide DA7R. *Acta Pharm Sin B* 2018;**8**:106–15.

48. Liu R, Hu C, Yang Y, Zhang J, Gao H. Theranostic nanoparticles with tumor-specific enzyme-triggered size reduction and drug release to perform photothermal therapy for breast cancer treatment. *Acta Pharm Sin B* 2019;**9**:410–20.

49. Ware MJ, Keshishian V, Law JJ, Ho JC, Favela CA, Rees P, et al. Generation of an *in vitro* 3D PDAC stroma rich spheroid model. *Biomaterials* 2016;**108**:129–42.

50. Zhou H, Fan Z, Deng J, Lemons PK, Arhontoulis DC, Bowne WB, et al. Hyaluronidase embedded in nanocarrier PEG shell for enhanced tumor penetration and highly efficient antitumor efficacy. *Nano Lett* 2016;**16**:3268–77.

51. Zhang Z, Wang X, Li B, Hou Y, Yang J, Yi L. Development of a novel morphological paclitaxel-loaded PLGA microspheres for effective cancer therapy: *in vitro* and *in vivo* evaluations. *Drug Deliv* 2018;**25**:166–77.